Measurement and analysis of optical surface properties for input to ShipIR

David A. Vaitekunas[a,1], Jim Jafolla[b,2], Paul McKenna[b], Martin Szczesniak[b]
[a]W.R. Davis Engineering Limited, 1260 Old Innes Road, Ottawa, Ontario, Canada K1B 3V3
[b]Surface Optics Corporation, 11555 Rancho Bernardo Rd., San Diego, CA, USA 92127

ABSTRACT

A new standard for the measurement and analysis of optical surface properties for input to the ShipIR model (Vaitekunas, 2002) are developed and tested using paint specimens taken from the unclassified Canadian research vessel (CFAV Quest). The theory and equations used to convert the in-lab and in-field surface property measurements into ShipIR model input parameters are described. The resultant data consists of two thermal model input parameters, solar absorptivity (α_s) and thermal emissivity (ε_T); and a series of in-band surface properties, the nominal emissivity (ε), nominal specular reflectance (ρ_S), angular lobe-width (*e*) and a grazing-angle (*b*) parameter. The original measurements in 2004 were supplemented with new hemispherical directional reflectance (HDR) and bi-directional reflectance distribution function (BRDF) measurements in 2008 to track the changes in the paint specimens and expand the analysis for additional input parameters to ShipIR. A more rigorous treatment of the BRDF model relates the HDR and BRDF measurements to a single surface roughness parameter (σ). In-field measurements performed using the SOC-410 hand-held reflectometer also provides a measurement of any spatial variation in HDR, a round-robin basis of comparison between the in-lab and surrogate in-field measurement of surfaces that can't be sent in for in-lab measurement.

Keywords: optical surface properties, surface radiance model, thermal model, measurements

1. INTRODUCTION

The methods and procedures used by W.R. Davis Engineering Ltd (Davis) to analyse a series of optical surface property measurements performed by the Surface Optics Corporation (SOC) on two paint samples from the unclassified Canadian research vessel CFAV Quest (Vaitekunas, 2004) are described. The main objective is to define a standard set of measurements and analysis procedures to obtain the inputs required by the thermal and in-band radiation models of ShipIR (Vaitekunas, 2002) with an adequate level of detail and accuracy. By considering two unclassified navy paints on an unclassified ship, the results of this research can be shared within the infrared modelling community and serve as a template for other users who need to perform a similar measurement of their own surface coatings. Some of the methods and results were presented at an earlier workshop (Vaitekunas, 2006), however new additions include the HDR at higher angles of incidence (θ=50–80°), BRDF measurements at 4 and 10 μm and 20° and 30°, and an expanded set of probability density Function (PDF) reflectance equations used to obtain the lobe-width angle (*e*) and grazing angle coefficient (*b*) used in the Sandford and Robertson (1985) model.

[1] dvaitekunas@davis-eng.com; http://www.davis-eng.com; phone: +1 613 748 5500; fax: +1 613 748 3972

[2] jjafolla@surfaceoptics.com; http://www.surfaceoptics.com.com; phone: +1 858 675 7404; fax: +1 858 675 2028

2. IN-LAB MEASUREMENTS

Based on discussions following the 2006 ITBM&S workshop, the following set of optical property measurements were defined as a minimum for any new surface coating being added to ShipIR:

- hemispherical directional reflectance (HDR) from 0.3 to 50 μm, using a collimated source at 20° incidence,
- Diffuse directional reflectance (DDR) from 0.3 to 26 μm, using a collimated source at 20° incidence,
- HDR measurements from 0.3 to 26 μm, using a collimated source at 50°, 60°, 70°, and 80° incidence,
- Bi-directional reflectance distribution function (BRDF) measurements at 4.0 and 10.0 μm for an incident source angle of 20° or 30° and reflection angles varying from -85° to +85°, in-plane with the source.

The 0.3 to 50 μm HDR measurements are used to compute the solar absorptivity and thermal emissivity of the surface. The 0.3 to 26 μm HDR and DDR measurements define the diffuse reflectance and provide a first estimate of the nominal specular reflectance (NSR). Additional 0.3 to 26 μm HDR measurements at 50–80° are used to calculate the gazing angle (*b*) parameter in the Sandford and Robertson (1985) model. The diffuse and specular reflectance values at 4.0 and 10.0 μm are combined with the two BRDF measurements to derive a surface roughness (σ) and lobe-width angle (*e*) for the surface. The definition of these variables and their extraction from the surface property measurement data are described in the sub-sections to follow. Some of the original 2004 paint measurements were repeated by SOC to determine if the paint specimens had changed while in storage, and to verify that the theory applies equally well to measurements taken at 20° and 30° incidence.

2.1 Thermal Property Analysis

The thermal property analysis uses the 0.3 to 50 μm HDR data at 20° or 30° to define two important thermal radiation model parameters, the solar absorptivity (α_s) and the thermal emissivity (ε_T). The entire wavelength spectrum is divided into two mutually exclusive bands, the optical or solar band and the earth-bound or thermal band:

$$\alpha_S = 1 - \frac{\int_0^\infty \rho_{hdr}(\nu) E_{sun}(\nu) d\nu}{\int_0^\infty E_{sun}(\nu) d\nu} \qquad \textbf{(1)}$$

$$\varepsilon_T = 1 - \frac{\int_0^\infty \rho_{hdr}(\nu) E_{bck}(\nu) d\nu}{\int_0^\infty E_{bck}(\nu) d\nu} \qquad \textbf{(2)}$$

These two properties are used by the ShipIR thermal model to compute the net radiative heat flux on each surface facet, and predict the resultant platform surface temperature(s), including the multi-bounce effects of low-emissivity (low-ε) and low solar absorptive (LSA) surfaces. Previous model verification studies have shown that not segregating the multi-bounce radiation form these two wave-bands can result in significant under-predictions of surface temperature and thermal signature. Figures 1 and 2 show the HDR measurements of the white Quest paint plotted against the two sample background emission spectrum, the sun (E_{sun}) and thermal sky (E_{bck}). Similar plots are shown in Figures 3 and 4 for the yellow Quest paint. The resultant thermal properties are shown in Table 1, compared against the 2004 SOC measurements and the US Naval Research Laboratory (US-NRL) measurements prior to the NATO SIMVEX trial in 2001 (Fraedrich et al., 2004).

Table 1: Thermal property analysis of Quest white and yellow paint.

Measurement / Sample	White Paint		Yellow Paint	
	α_s	ε_T	α_s	ε_T
SIMVEX (2001)†	0.21	0.94	0.63	0.93
SOC (2004)	0.21	0.93	0.54	0.96
SOC (2008)	0.25	0.93	0.54	0.95

†based on an earlier paint sample (different paint supply).

These results show how the visual reflectance of the white paint in 2004 has decreased over time to produce a .04 increase in solar absorptivity, whereas the thermal emissivity remains unchanged. The diffuse directional reflectance (DDR) of the white paint, also plotted in Figures 1 and 2, shows no change between 2004 and 2008 for the 2–26 μm region. Similarly, no significant changes were noted in the yellow paint; only a .01 decrease in thermal emissivity is observed in Table 1. With no change in the yellow paint HDR, the DDR measurements were not repeated in 2008.

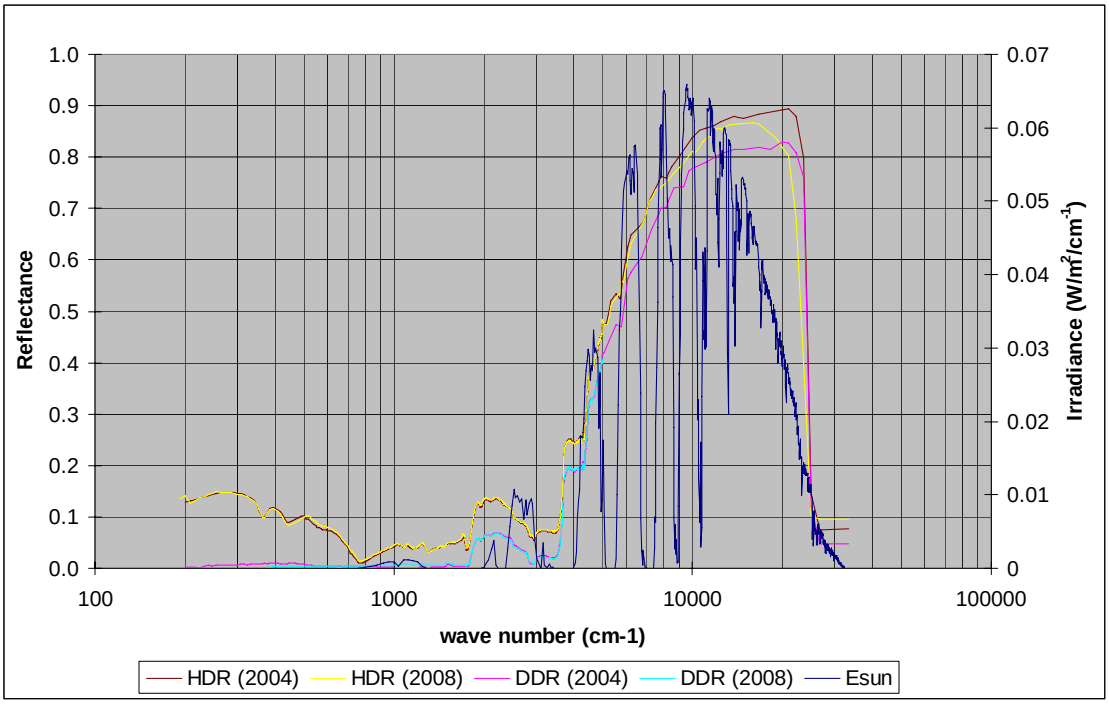

Figure 1: Various HDR and DDR measurements plotted against the solar emission (Esun) for the white paint.

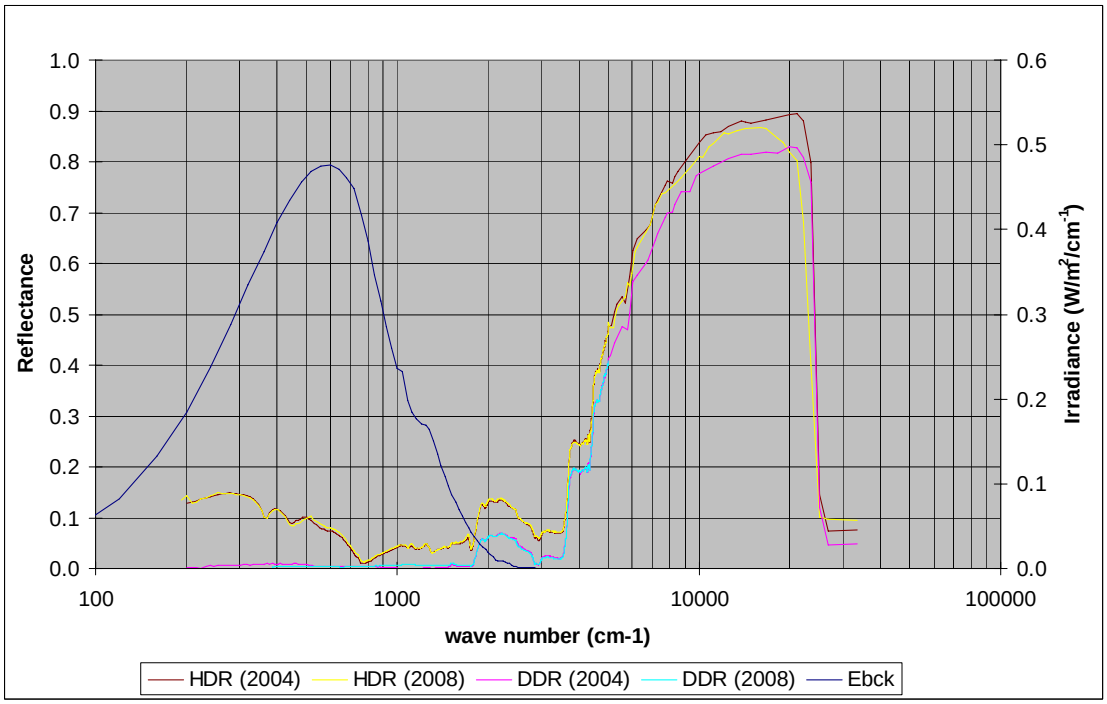

Figure 2: Various HDR and DDR measurements plotted against the thermal background emission (Ebck) for the white paint.

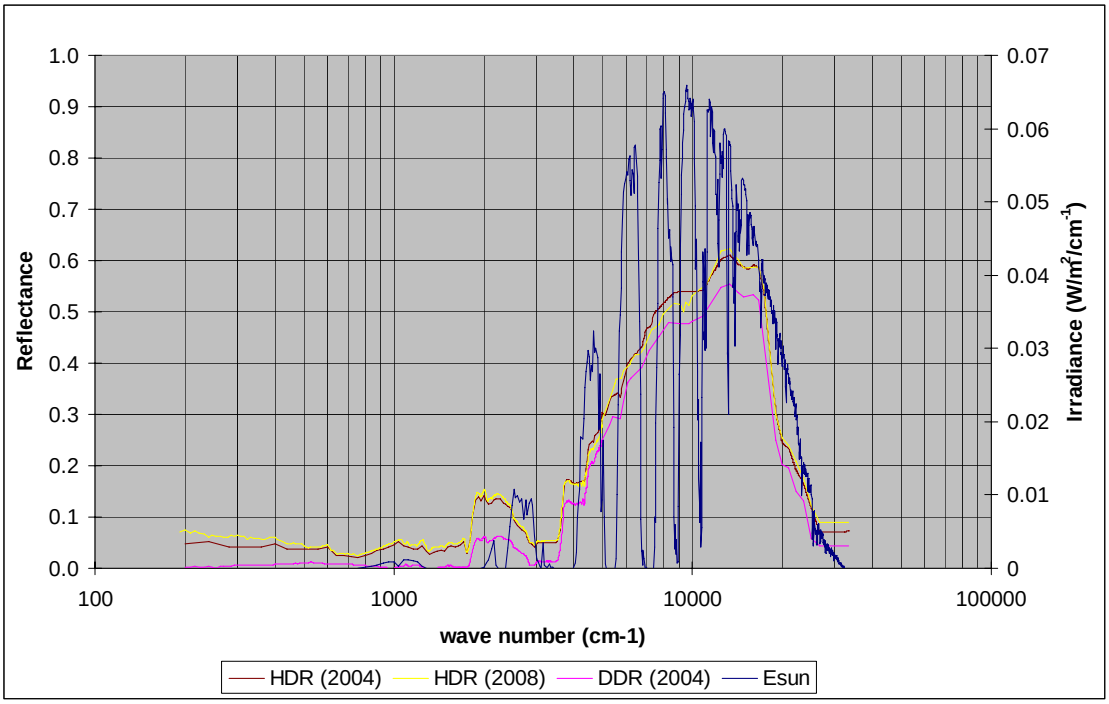

Figure 3: Various HDR and DDR measurements plotted against the solar emission (Esun) for the yellow paint.

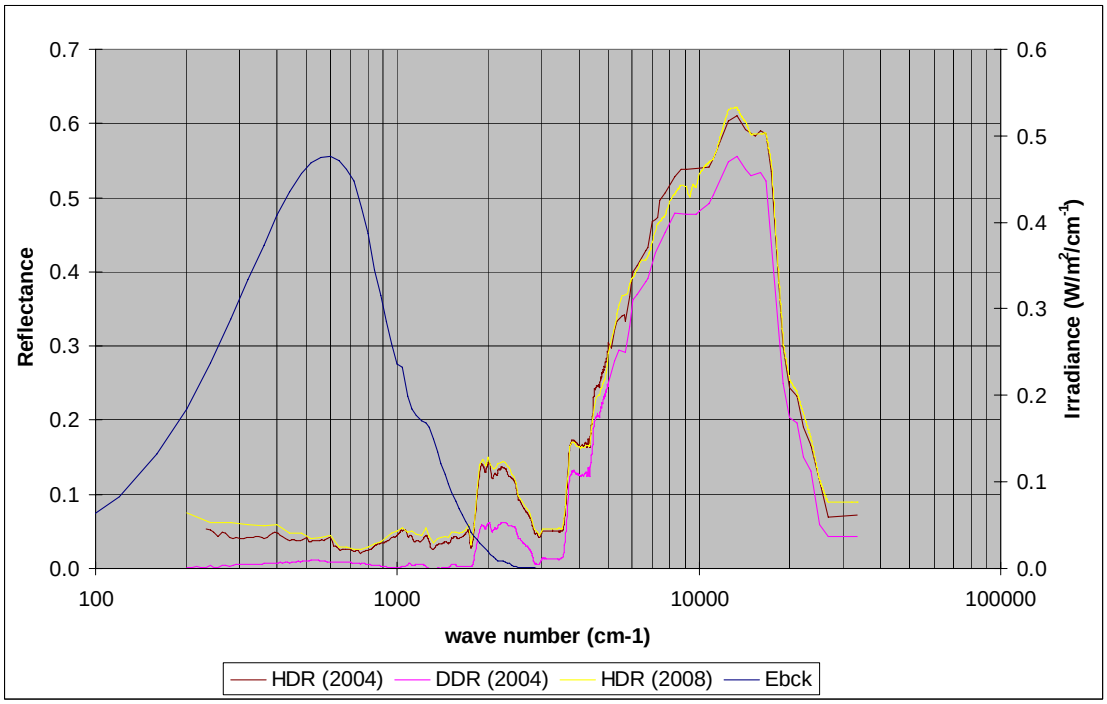

Figure 4: Various HDR and DDR measurements plotted against the thermal background emission (Ebck) for the yellow paint.

2.2 In-Band Directional Reflectance Model Analysis

The in-band directional HDR measurements versus angle data are used to derive a grazing angle coefficient (*b*) for the ShipIR model, which describes the variation in surface reflectance with incidence angle (θ). The total reflectance is assumed to be the summation of diffuse-only (ρ_D) and specular-only (ρ_S) components:

$$\rho(\theta,\lambda) = \rho_D(\lambda) + \rho_S(\theta,\lambda) \quad \textbf{(3)}$$

The angular variation in surface reflectance is assumed to be completely specular and independent of spectrum, as postulated by Sandford and Robertson (1985):

$$\rho_S(\theta,\lambda) = g(\theta)\cdot\rho_S(0,\lambda) + [1-g(\theta)]\cdot[1-\rho_D(\lambda)] \quad \textbf{(4)}$$

The functional form of *g* proposed by Sandford and Robertson (1985) model:

$$g(\theta) = \frac{1}{1+b_{SR}^2\cdot\tan^2\theta} \quad \textbf{(5)}$$

results in an asymptotic total reflectance value of unity at 90° incidence (grazing angle). There is a small discrepancy between the *b* value used by ShipIR and that of Sandford-Robertson (1985):

$$b_{ShipIR} = b_{SR}^2 \quad \textbf{(6)}$$

The first step in estimating *b* is to compute the following normalized reflectance ratio (ρ*):

$$\rho^*(\theta) = \frac{\rho_S(\theta)-\rho_S(0)}{1-\rho_D-\rho_S(0)} = 1-g(\theta) \quad \textbf{(7)}$$

Based on the measured HDR=ρ(θ), the DDR=ρ_D, the specular reflectance $\rho_S(\theta)$ and nominal specular reflectance, NSR=$\rho_S(0)$, are computed from Equations (3) and (4). The HDR for different incidence angles (θ) of the Quest white paint are shown in Figure 5. The resultant specular reflectance (SR) and normalized reflectance ratio (ρ*) are shown in Figures 6 and 7, respectively; comparable data were obtained for the yellow paint. As described by Equation (5), the HDR, SR, and ρ* follow an asymptotic function towards unity at the grazing angle (90°). If the angular and spectral variations in SR are truly separable, the curves in Figure 7 should all be horizontal (constant) versus wave number, since *g* is only a function of *b* and θ. Although the curves share a consistent pattern versus wave number, the deviation from an average value provide an early

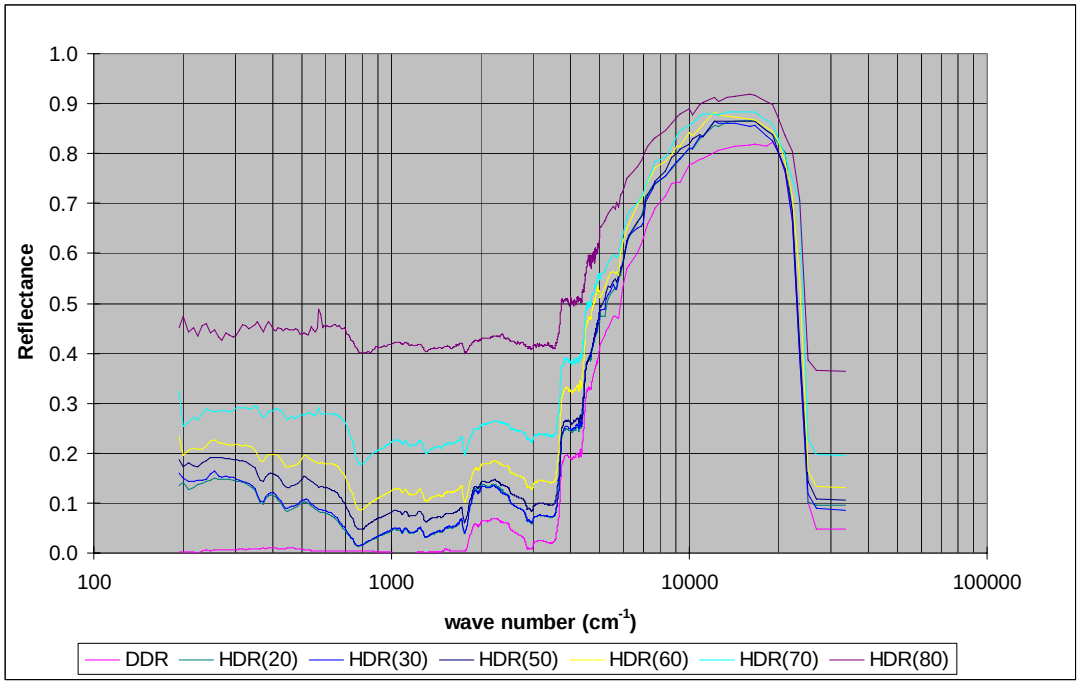

Figure 5: Measured DDR and HDR at 20° co-plotted against the additional HDR at 30°, 50°, 60°, 70° and 80° for the Quest white paint.

indication that the residual error between the Sandford-Robertson model and the measurement is not negligible.

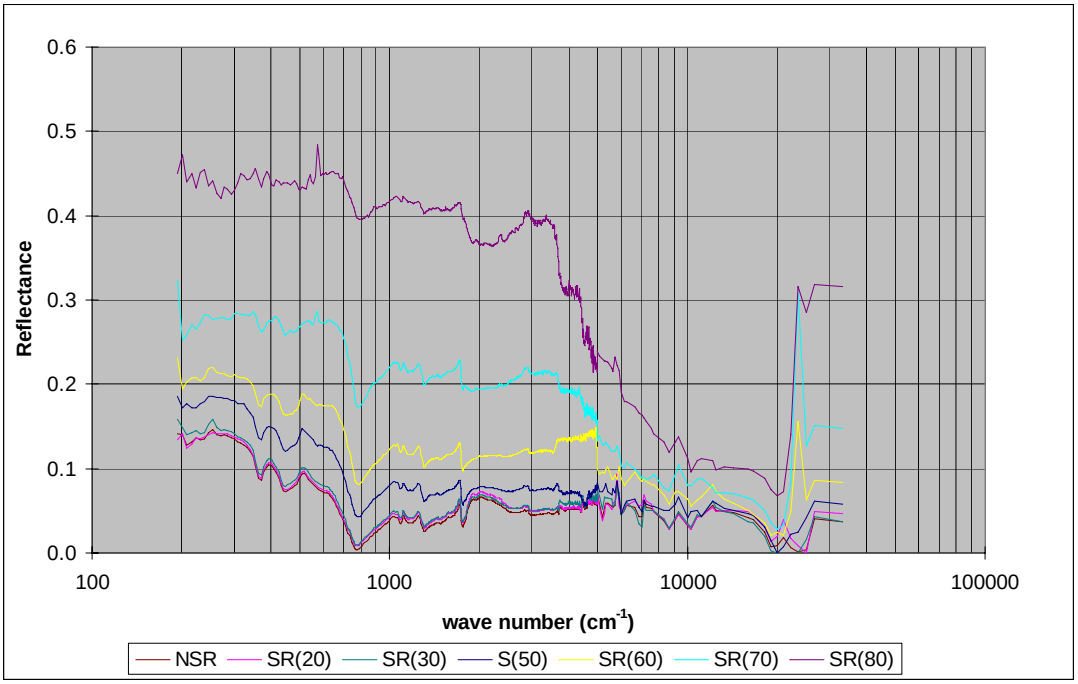

Figure 6: Calculated specular reflectance (SR) at 0°, 20°, 30°, 50°, 60°, 70° and 80° for the Quest white paint.

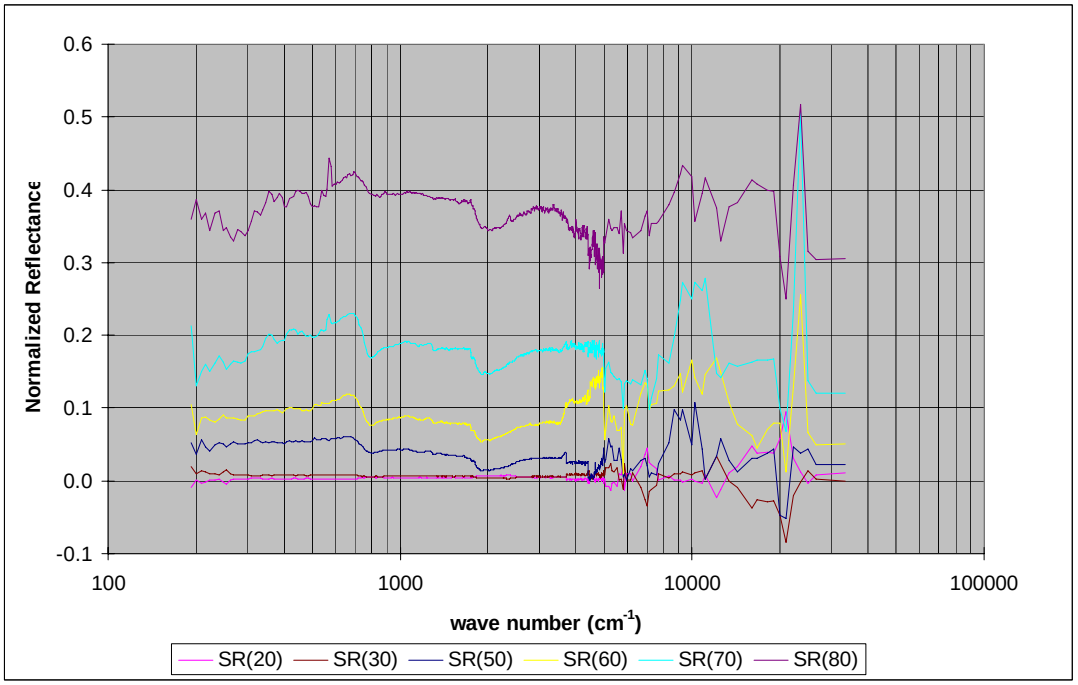

Figure 7: Normalized reflectance of the Quest white paint at 20°, 30°, 50°, 60°, 70° and 80° incidence.

The next step involves the calculation of a suitable *b* value so that the average error in ρ* is zero. This is done using a spreadsheet to calculate the difference between the measured data in Figure 7 and Equation (5) for a specified range of interest; 2.5 to 26 μm was used for the white paint and 5.9 to 29 μm was used for the yellow paint. The resultant *b*-curves for the white and yellow paints are shown in Figures 8 and 9, respectively. Nearly identical values of b_{ShipIR} are obtained for the white (0.0229) and yellow (0.0226) paints. The overall error in the SR model is shown in Figures 10 and 11, plotting predicted values from Equation (4) versus measured SR at every wavelength. Although the average value is zero, over the spectral range specified, the residuals (2σ) range from 5.4%for the white paint to 8.4% for the yellow paint.

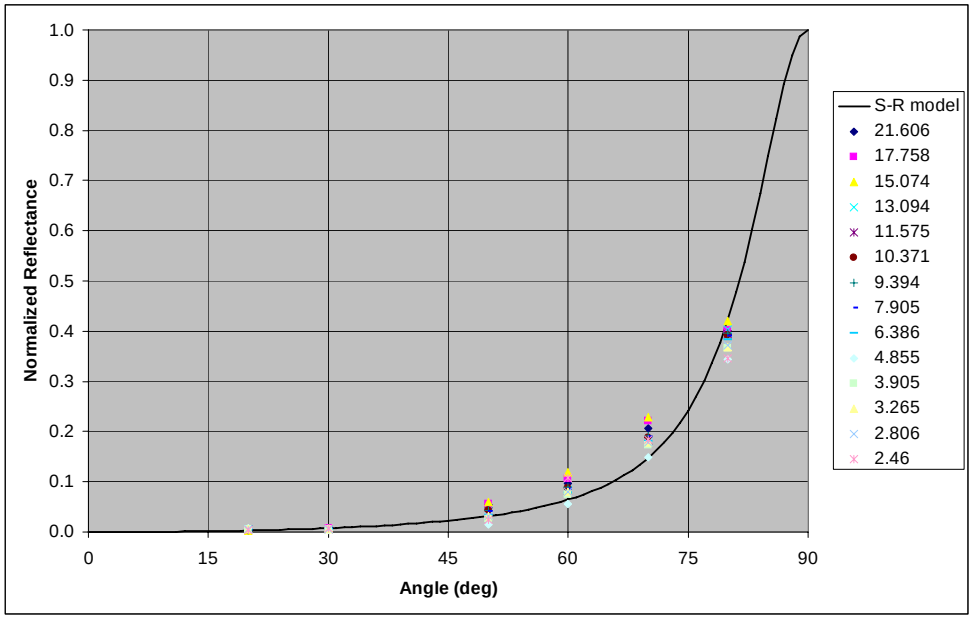

Figure 8: Predicted and measured ρ* versus angle at various wavelengths for the Quest white paint.

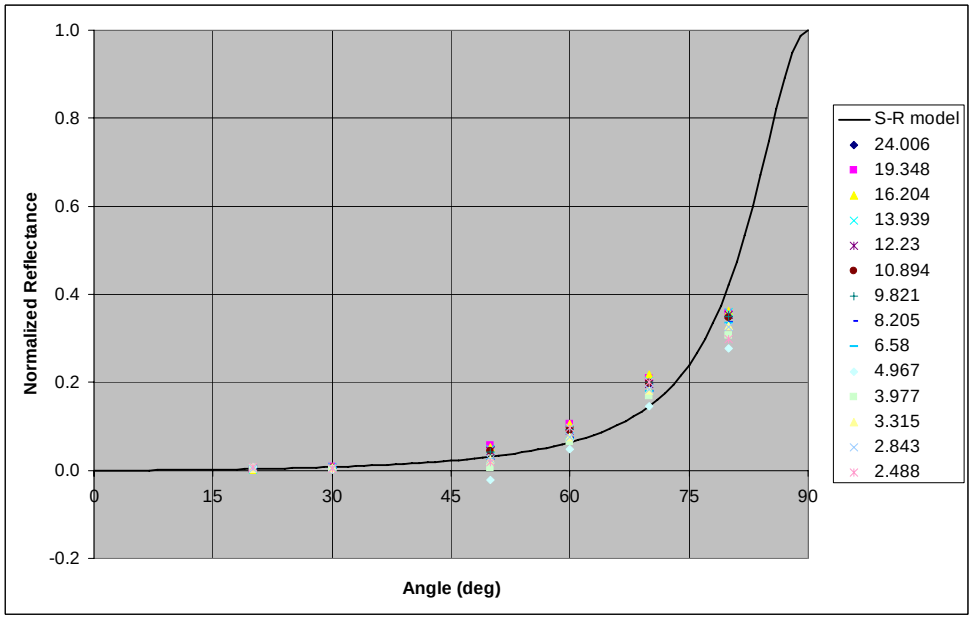

Figure 9: Predicted and measured ρ* versus angle at various wavelengths for the Quest yellow paint.

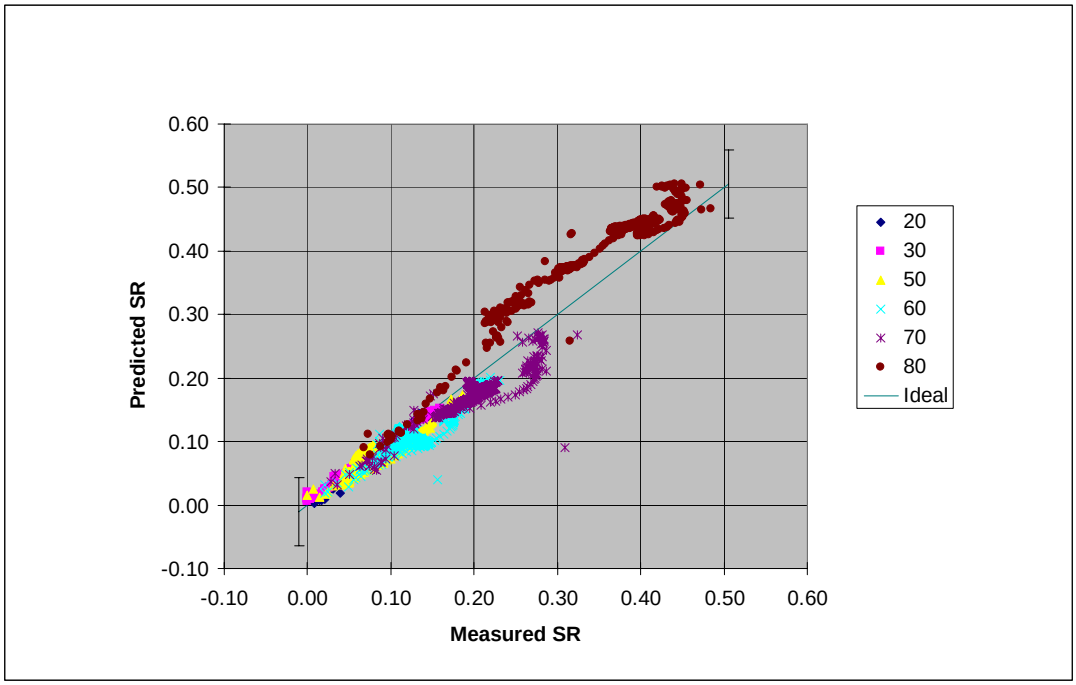

Figure 10: Predicted versus measured specular reflectance (SR) for the Quest white paint at different angles of incidence.

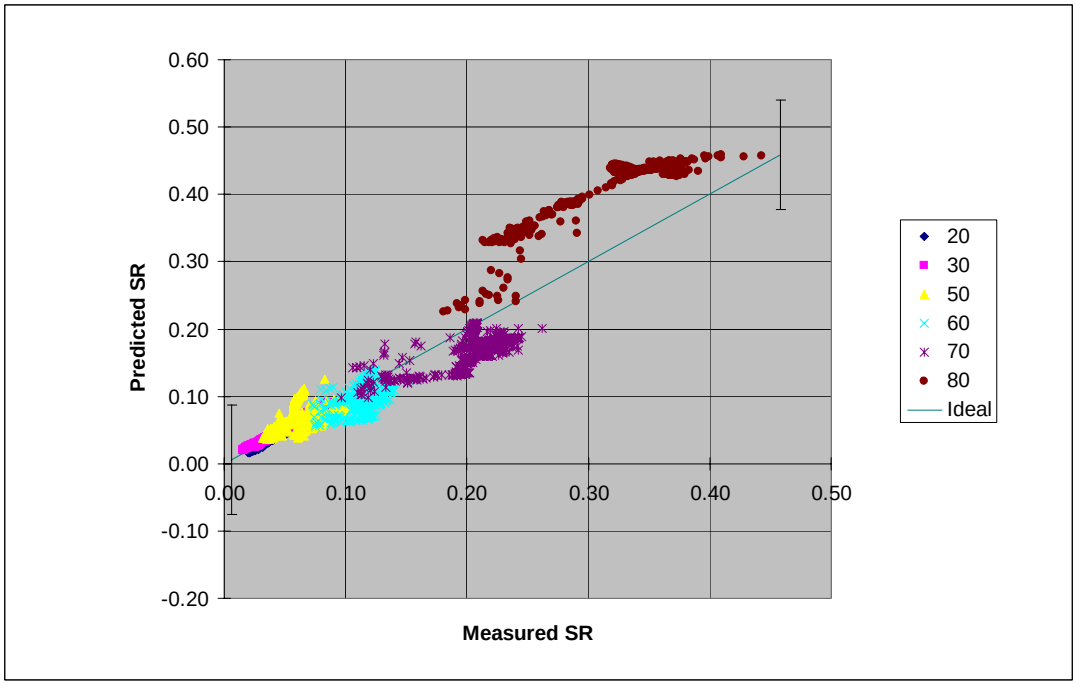

Figure 11: Predicted versus measured specular reflectance (SR) for the Quest yellow paint at different angles of incidence.

2.3 Surface Roughness and Specular Lobe-Width Angle

An important geometrical parameter affecting the sun-glint reflections off the ship is the surface roughness (σ) or lobe-width angle (*e*) of the surface. This value is obtained by measuring the in-plane BRDF at different reflection angles relative to one incident source angle (20° or 30°) at two different infrared wavelengths (4-μm and 10-μm). The results for the Quest white and yellow paints are shown in Figures 12 through 15. Two different models are compared to the measurement, a Gaussian probability density function (PDF) model of surface roughness and the more traditional Standford-Robertson approximation (FWHM).

A Gaussian slope statistic model has been developed (Vaitekunas, 2006) based on the methods employed by Cox and Munk (1954) to model the sun-glint reflections off the ocean surface. The resultant energy equation for a small point source reflection off an isotropic Gaussian roughened surface ($\sigma_x=\sigma_y=\sigma$) is given by the following energy integral:

$$L_r(\phi_r,\theta_r) = \int_{\Omega_i} \rho_s(\mu)\, p(m_x,m_y)\, L_i(\phi_i,\theta_i)\, dm_x\, dm_y \qquad \textbf{(8)}$$

where

$$p(m_x,m_y) = \frac{1}{2\pi\sigma^2}\exp\left[\frac{-(m_x^2+m_y^2)}{2\sigma^2}\right] \qquad \textbf{(9)}$$

is the probability density of a specific surface slope. Because of the small angle subtended by the source, the specular reflectance and the probability density for the source reflection don't change over the domain of the above integral (Ω_i):

$$\begin{aligned} L_r(\phi_r,\theta_r) &= \rho_s(\mu)\, p(m_x,m_y)\, L_i(\phi_i,\theta_i) \int_{\Omega_i} dm_x\, dm_y \\ &= \rho_s(\mu)\, p(m_x,m_y)\, L_i(\phi_i,\theta_i) A_s \end{aligned} \qquad \textbf{(10)}$$

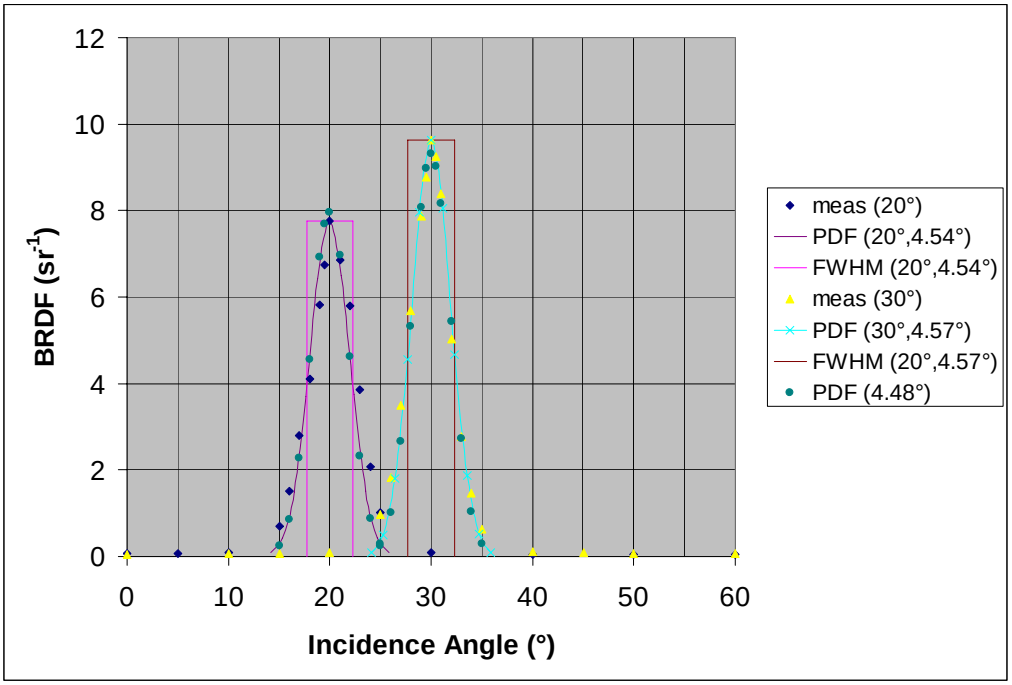

Figure 12: BRDF measurements of the Quest white paint at 4 microns (20°, 30°).

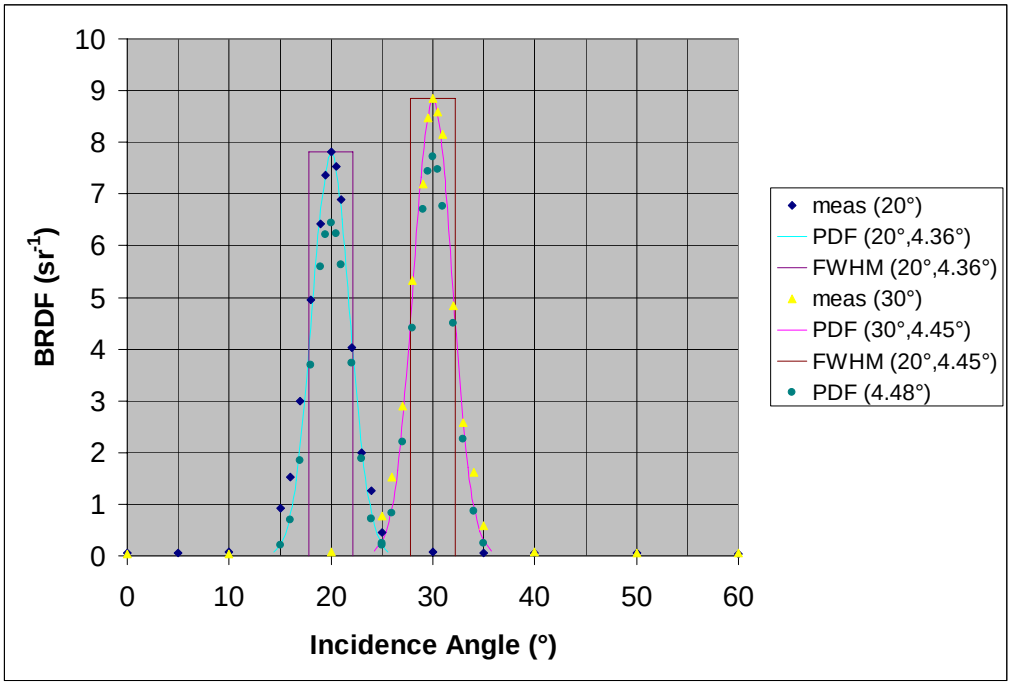

Figure 13: BRDF measurements of the Quest white paint at 10 microns (20°, 30°).

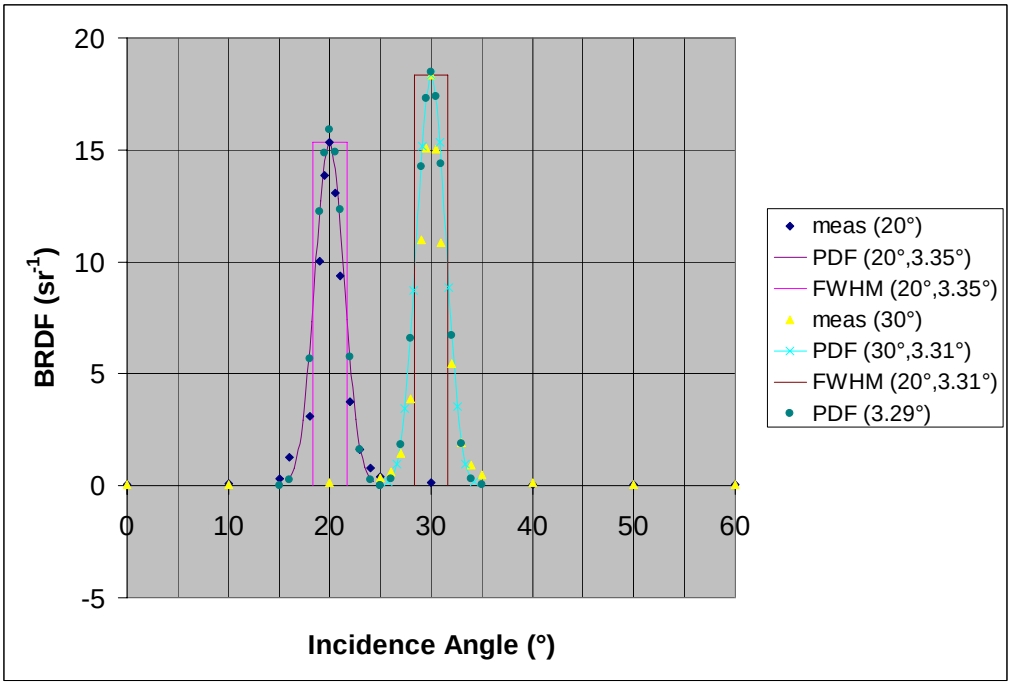

Figure 14: BRDF measurements of the Quest yellow paint at 4 microns (20°, 30°).

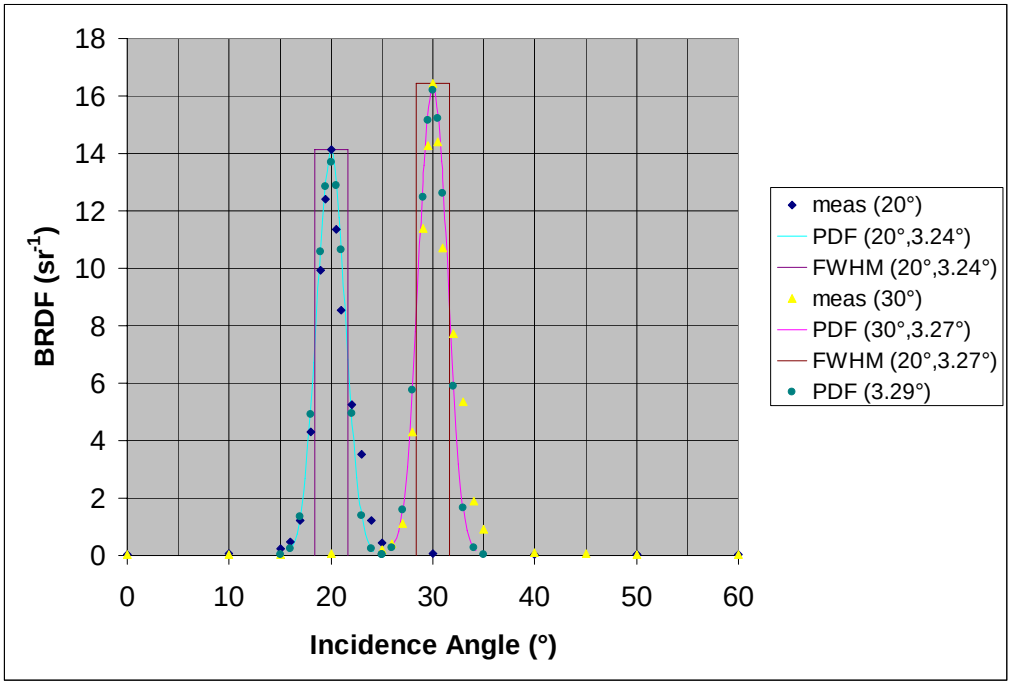

Figure 15: BRDF measurements of the Quest yellow paint at 10 microns (20°, 30°).

(m_x,m_y) are the slope values computed along the line-of-sight to the centre of the source, and A_s is the slope-area subtended by an incident ray tracing the periphery of the source. Because the BRDF measurements are performed in-line with the source ($\phi_r=\phi_i+\pi$), the transverse slopes to the centre of the source are zero ($m_y=0$), and because the incident source angle is fixed during these BRDF measurements (θ_i=20° or 30°), the following simplifications are introduced to define the centre line surface slope (m_x):

$$m_x = \tan(\mu) \qquad \mu = \frac{|\theta_r - \theta_i|}{2} \tag{11}$$

Hence,

$$L_r(\phi_r,\theta_r) = \rho_s(\mu)\frac{1}{\sigma\sqrt{2\pi}}p(m_x)L_i(\phi_i,\theta_i)A_s \tag{12}$$

where

$$p(m_x) = \frac{1}{\sigma\sqrt{2\pi}}\exp\left[\frac{-\tan^2(\mu)}{2\sigma^2}\right] \tag{13}$$

Recalling the definition of BRDF (sr^{-1}):

$$BRDF = \frac{L_r(\phi_r,\theta_r)}{E_i(\phi_i,\theta_i)} = \frac{L_r(\phi_r,\theta_r)}{L_i(\phi_i,\theta_i)\cdot\omega_s} = \rho_s(\mu)\frac{1}{\sigma\sqrt{2\pi}}p(m_x)\frac{A_s}{\omega_s} \tag{14}$$

we now have two unknowns, the slope-area integral (A_s) and the surface roughness (σ). The slope-area integral is difficult to solve analytically, so it is normally obtained numerically by mapping discrete values of (m_x,m_y) around the periphery of the source and computing the resultant slope-area integral using a finite difference integral. The resultant values are proportional to the size of the source (ω_s), so that the ratio (A_s/ω_s) are tabulated as a function of (θ_i,θ_r) in Table 2. Further analysis has shown that changes in (A_s/ω_s) are less than 0.1% for point sources ranging in size from 0.25° to 5° aperture. With values of (A_s/ω_s), the surface roughness is computed directly from the peak value of BRDF at $\theta_i=\theta_r$ ($m_x=m_y=0$) using:

$$BRDF_{\max} = \frac{\rho_s(\theta_i)}{2\pi\sigma^2} \cdot \frac{A_s}{\omega_s} \quad \textbf{(15)}$$

$$\sigma = \sqrt{\frac{\rho_s(\theta_i)}{2\pi \cdot BRDF_{\max}} \cdot \frac{A_s}{\omega_s}} \quad \textbf{(16)}$$

The full-width at half-maximum (FWHM) is also calculated from the PDF using the slope value at 50% of the peak BRDF value:

$$BRDF_{1/2} = \frac{\rho_s(\mu_{1/2})}{\sigma\sqrt{2\pi}}\, p(m_x)\frac{A_s}{\omega_s} = \frac{1}{2} \cdot BRDF_{\max} = \frac{\rho_s(\theta_i)}{2\pi\sigma^2} \cdot \frac{A_s}{\omega_s} \quad \textbf{(17)}$$

assuming:

$$\rho_s(\mu_{1/2}) \approx \rho_s(\mu_0) \qquad \frac{A_s(\mu_{1/2})}{\omega_s} \approx \frac{A_s(\mu_0)}{\omega_s} \quad \textbf{(18)}$$

The resultant slope at the FWHM is now defined as:

$$p(m_x) = \frac{1}{2} \cdot \frac{1}{\sigma\sqrt{2\pi}} \quad \textbf{(19)}$$

Comparing Equations (13) and (19):

$$\exp\left[\frac{-\tan^2(\mu_{1/2})}{2\sigma^2}\right] = \frac{1}{2}$$

$$\frac{-\tan^2(\mu_{1/2})}{2\sigma^2} = \ln(1/2) \quad \textbf{(20)}$$

$$\mu_{1/2} = \tan^{-1}\left[\sigma\sqrt{-2\ln(1/2)}\right] = \frac{\theta_{1/2} - \theta_i}{2}$$

Hence,

$$FWHM = 2\left(\theta_{1/2} - \theta_i\right) = 4\tan^{-1}\left(\sigma\sqrt{-2\ln(1/2)}\right) \quad \textbf{(21)}$$

The value of surface roughness (σ) obtained for each BRDF measurement are shown as a lobe-width angle in the legend of Figures 12 through 15. An average lobe-width of 4.48° and 3.29° was found for the white and yellow paints, respectively. These average values were reinserted into the PDF model to predict a BRDF value for each measurement point, the results of which are also shown in Figures 12 through 15 (PDF curve). The average error (μ) and standard deviation (σ) in BRDF are summarized in Table 3. The standard deviation of 5–10% is attributed to the large gradient in BRDF (as a function of reflection angle), making it very sensitive to any uncertainty in the angle control of the reflectometer. A summary of the measured and calculated properties of the BRDF model are shown in Table 4. The results show how the increase in BRDF between incidence angles of 20° and 30° is not only the result of increased specular reflectance (versus angle) but also the result of increases in (A_s/ω_s):

- the peak BRDF increases by 20–24% at 4 μm, and 13–16% at 10 μm, between 20° to 30°,
- 7–8% of the increase at 4 μm and 9–11% at 10 μm is due to specular reflectance,
- the remaining 8.5% is attributed to slope-area (A_s/ω_s) change (independent of reflectance and wavelength).

Table 2: A_s/ω_s for the two incident angles used to measure BRDF.

$\theta_i = 20°$		$\theta_i = 30°$	
θ_r	A_s/ω_s	θ_r	A_s/ω_s
15°	0.2629	25°	0.2827
16°	0.2634	26°	0.2837
17°	0.2639	27°	0.2848
18°	0.2645	28°	0.2860
19°	0.2653	29°	0.2873
19.5°	0.2656	29.5°	0.2880
20°	0.2661	30°	0.2887
20.5°	0.2665	30.5°	0.2895
21°	0.2669	31°	0.2902
22°	0.2679	32°	0.2919
23°	0.2690	33°	0.2936
24°	0.2701	34°	0.2954
25°	0.2714	35°	0.2974

Table 3: Statistical error between the predicted and measured BRDF, as a fraction of the peak BRDF, for the 4 and 10 micron data sets (both incidence angles).

Paint	λ = 4 μm		λ = 10 μm	
	μ	σ	μ	σ
white	-0.030	0.080	-0.099	0.048
yellow	0.065	0.093	-0.001	0.085

Table 4: Comparison of measured Reflectance and BRDF values between the Quest white and yellow paints.

Data Set		White (FWHM=4.48°, σ=0.0166)				Yellow (FWHM=3.29°, σ=0.0122)			
		ρ_S	ρ_D	BRDF	A_s/ω_s	ρ_S	ρ_D	BRDF	A_s/ω_s
4 μm	20°	0.0519	0.0491	7.764	.2661	0.0559	0.0447	15.34	.2661
	30°	0.0560		9.639	.2887	0.0600		18.35	.2887
10 μm	20°	0.0420	0.0010	7.807	.2661	0.0482	0.0004	14.12	.2661
	30°	0.0464		8.855	.2887	0.0525		16.43	.2887

3. IN-FIELD MEASUREMENTS

A series of in-field measurements were performed by Davis onboard Quest using the SOC-410 handheld Directional Hemispherical Reflectometer, as shown in Figure 16. This unique instrument developed by Surface Optics provides a quick, unobtrusive, and accurate method of measuring HDR at 20° and 60° in six (6) different optical and thermal wave bands. The purpose of these measurements is to:

- perform a round robin verification of the white and yellow HDR, by comparing the SOC-410 in-band measurements with the full-spectral in-lab measurements from the SOC-100,
- adapt the techniques used to post-process the SOC-100 measurements to the in-band SOC-410 results and obtain a limited set of inputs to the ShipIR model for areas of the ship where paint specimens cannot be collected for in-lab measurement.

Figure 16: SOC-410 handheld directional hemispherical reflectometer.

Figure 17 shows the ease-of-use of this portable HDR instrument. The user simply puts the opening of the reflectometer up against a surface to be measured, and presses down on the trigger until an audible click is heard indicating the direct measurement is complete. To finalize the measurement, the user takes a sample background measurement by pointing the device towards an open area and presses the trigger, as shown in Figure 18, until the same audible click is heard. A number of samples for the same coating type, taken from different areas of the ship are saved to the same output file on the compact flash data card used for later retrieval and analysis.

Figure 17: Direct sample using SOC-410.

Figure 18: Background sample using SOC-410.

3.1 Thermal Model Properties

To compare the in-band measurements from the SOC-410 with the full-spectral HDR measurements from the SOC-100, knowledge of the spectral response for each wave band sensor/filter in the SOC-410 is required; these are co-plotted with the 2004 HDR measurements of the Quest white and yellow paints versus wave number in Figure 19. The full-spectral and in-band HDR are related by the following spectral response integral:

$$HDR_{410} = \frac{\int_0^\infty \tau_{SRF}(\nu) HDR_{100}(\nu) d\nu}{\int_0^\infty \tau_{SRF}(\nu) d\nu} \quad \textbf{(22)}$$

Table 5 summarizes the above integral for the two Quest paints in the six SOC-410 wave bands, and compares the differences between the two measurements against the mean and standard error in the 20 and 18 SOC-410 samples taken of the white and yellow paints, respectively. In all but four cases the absolute difference between the two methods is larger than the twice the standard error in the SOC-410 samples, with differences ranging from 0.5% to 7%. Possible causes for the large discrepancy include inaccuracies in the SRF specified, differences in the paint samples, operator error (e.g., proper usage of the specular gold calibration coupon). It should be noted that the 2004 and 2008 SOC-100 HDR measurements were performed on a specimen prepared in the workshop during 2004; the SOC 410 measurements were taken onboard the actual ship during a Quest measurement trial held during May 2007.

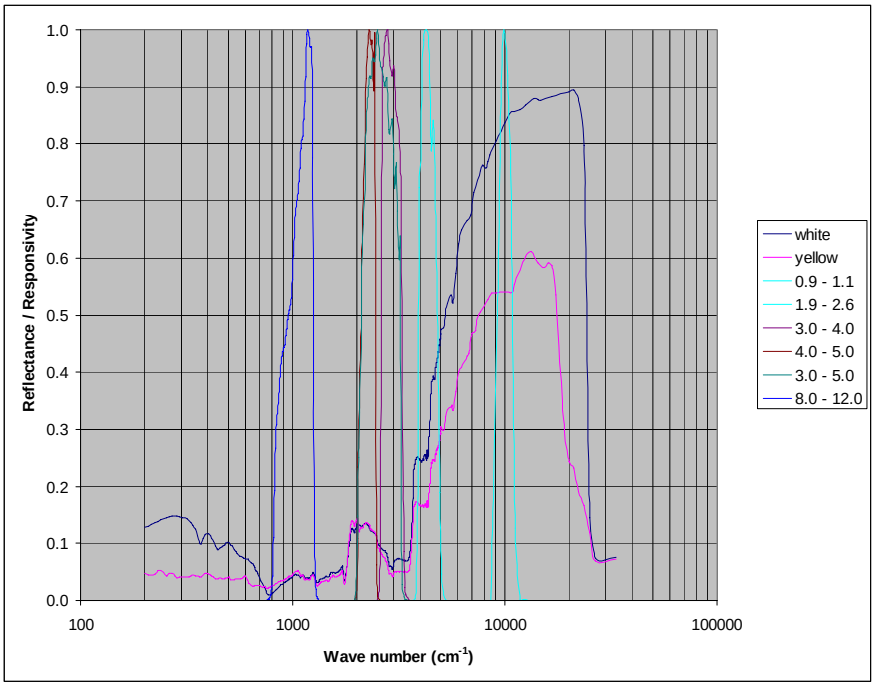

Figure 19: Spectral response curves for the SOC-410 co-plotted against the full-spectral HDR curves for the Quest white and yellow paints.

The next step involves the estimation of two important thermal model input parameters, the solar absorptivity (α_S) and thermal emissivity (ε_T), using the nominal SOC-410 HDR measurements at 20°. A set of normalized weighting factors are first derived from the spectral integration of a typical solar emission spectrum across the spectral response of each (i^{th}) sensor band:

$$E_{sun,i} = \int_0^\infty \tau_{SRF,i}(\nu) E_{sun}(\nu) d\nu \qquad \textbf{(23)}$$

The results from the most relevant wave bands are then weighted against the sum:

$$W_{S,i} = \frac{E_{sun,i}}{\sum_i^{N_b} E_{sun,i}} \qquad \textbf{(24)}$$

and used to estimate the solar absorptivity. The same procedure is repeated for the typical thermal (sky) background emission spectrum:

$$E_{bck,i} = \int_0^\infty \tau_{SRF,i}(\nu) E_{bck}(\nu) d\nu \qquad \textbf{(25)}$$

$$W_{T,i} = \frac{E_{bck,i}}{\sum_i^{N_b} E_{bck,i}} \qquad \textbf{(26)}$$

The resultant weighting factors are shown in Table 6. Only the 0.9-1.1, 1.9-2.6 and 3.0-5.0 wave-bands are used to estimate the solar absorptivity, and the 3.0-5.0 and 8.0-12.0

Table 5: Comparison of nominal HDR measurements

Band	SOC-410		SOC-100	Absolute Difference
	mean	std. error	integral	
Quest white paint				
0.9 - 1.1	0.882	1.0%	0.835	4.7%
1.9 - 2.6	0.322	0.7%	0.315	0.7%
3.0 - 4.0	0.060	0.2%	0.073	-1.3%
4.0 - 5.0	0.064	0.2%	0.127	-6.3%
3.0 - 5.0	0.069	0.2%	0.095	-2.6%
8.0 - 12.0	0.075	0.1%	0.039	3.6%
Quest yellow paint				
0.9 - 1.1	0.608	0.7%	0.541	6.7%
1.9 - 2.6	0.249	2.4%	0.204	4.5%
3.0 - 4.0	0.050	0.4%	0.056	-0.6%
4.0 - 5.0	0.069	1.4%	0.128	-5.9%
3.0 - 5.0	0.091	2.6%	0.087	0.5%
8.0 - 12.0	0.068	0.1%	0.041	2.7%

Note: errors and differences are in absolute reflectance (%)

wave-bands are used to estimate the thermal emissivity. The resultant properties for the Quest yellow and white paints are summarized in Table 7 along with the 2008 in-lab SOC-100 HDR integrals. The differences between the SOC-100 and SOC-410 thermal properties (0% to 7%) are similar to those obtained for the nominal in-band HDR. The fact the in-lab and in-field values match for the white paint is simply a coincidence; the actual HDR values used (see Table 5) vary by -6% and +5%.

Table 7 shows the thermal properties for other parts of the Quest that were not previously measured. For these surfaces, the solar absorptivity was previously estimated using digital colour photographs[3] and simply assume a high thermal emissivity (0.95). This was deemed sufficient for the NATO SIMVEX trial since most of the areas were small enough that they did not impact significantly on the overall ship signature. However two of the affected areas, the aluminum gangway on the port side (aluminum ladder) and the brown metal dumpster on the aft flight deck (brown bin), were found to be significant contributors to both the qualitative and quantitative signature of the Quest. The SOC-410-HDR measurements show that the original estimates of solar absorptivity were 13-14% too low. Further analysis is required to determine the net impact of these changes on the ShipIR model predictions of the Quest thermal infrared signature. This could be the topic of a future validation study. Other areas show an even larger difference between the original estimates and the in-field SOC-410 measurements. Both results illustrate the benefit of using the SOC-410-HDR during platform IR signature measurement trials. They can also complement the more detailed in-lab measurements by detecting changes in the paint associated with aging (UV exposure), repainting of the ship (different paint supply), or spatial variations in the surface reflectance around the ship; none of these can be derived from the in-lab measurements.

Table 6: Weighting factors used to estimate the solar absorptivity and thermal emissivity from the SOC-410 HDR measurements.

Band	E_{sun}		E_{bck}	
	W/m^2	Factor	W/m^2	Factor
0.9 - 1.1	77.163	0.7949	0.000	
1.9 - 2.6	15.131	0.1559	0.003	
3.0 - 4.0	3.129		0.392	
4.0 - 5.0	0.620		2.611	
3.0 - 5.0	4.776	0.0492	3.043	0.0454
8.0 - 12.0	0.229		64.027	0.9546

[3] RGB photographs were converted to greyscale; by fitting a straight-line to similar grey values from surfaces with measured HDR, a linear interpolation model was used to estimate solar absorptivity based on grey values from surfaces with no HDR measurements.

Table 7: Comparison of solar absorptivity and thermal emissivity obtained using the SOC-410 and SOC-100 HDR.

Material	Solar absorptivity (α_S)			Thermal Emissivity (ε_T)		
	SOC-100	SOC-410	Diff.	SOC-100	SOC-410	Diff.
white	0.25	0.25	0.0%	0.93	0.93	0.0%
yellow	0.54	0.47	-7.0%	0.95	0.93	-2.0%
Other Materials†	previous	SOC-410	Change	previous	SOC-410	Change
life-raft (white)	0.25	0.61	36.0%	0.93	0.96	3.0%
aluminum ladder	0.50	0.64	14.0%	0.95	0.92	-3.0%
black (anchor)	0.96	0.95	-1.0%	0.95	0.96	1.0%
brown bin	0.80	0.93	13.0%	0.95	0.95	0.0%
deck (smooth)	0.63	0.91	28.0%	0.95	0.96	1.0%
deck (no-slip)	0.63	0.68	5.0%	0.95	0.95	0.0%
door (wood)	0.50	0.42	-8.0%	0.90	0.93	3.0%
red locker (small)	0.80	0.37	-43.0%	0.95	0.93	-2.0%
red locker (large)	0.80	0.75	-5.0%	0.95	0.94	-1.0%
RHIB (red)	0.58	0.44	-14.0%	0.95	0.93	-2.0%
RHIB (black rubber)	0.96	0.95	-1.0%	0.95	0.98	3.0%
aluminum vent††	0.00	0.50	50.0%	0.00	0.66	66.0%
window	0.05	---	---	0.90	0.87	-3.0%

†Used in the ShipIR model but not measured; previous values were estimated from colour and measurements of other similar coatings.

††There are no entries in the current ShipIR (.mtl) file, in which case a zero value is assumed.

3.2 Surface Radiance Model Properties

The last step in the analysis of the SOC-410 HDR measurements is to estimate the nominal in-band emissivity and HDR at 0° incidence, and derive the grazing angle coefficient (*b*). The resultant *b* parameter is also used to determine whether the surface is DIFFUSE or SPECULAR[4]. Based on the theory presented in section 2.2, the following equations are used to calculate the HDR at 0° and the *b* parameter:

$$\rho^*(\theta) = \frac{\rho_S(\theta) - \rho_S(0)}{1 - \rho_D - \rho_S(0)} = \frac{HDR(\theta) - HDR(0)}{1 - HDR(0)} = 1 - g(\theta) \quad \textbf{(27)}$$

$$g(\theta) = \frac{1}{1 + b_{SR}^2 \cdot \tan^2\theta} \quad \Rightarrow \quad b = \frac{1 - g(\theta)}{g(\theta)} \cdot \frac{1}{\tan^2\theta} \quad \textbf{(28)}$$

$$HDR(0) = \frac{HDR(\theta) - \left[1 - g(\theta)\right]}{1 - \left[1 - g(\theta)\right]} = \frac{HDR(\theta) - \rho^*(\theta)}{1 - \rho^*(\theta)} \quad \textbf{(29)}$$

Equation (27) is computed at both 20° and 60°, using the HDR at 20° as an initial estimate for the HDR at 0°. Equation (28) is computed using an average value of *g* obtained from all six wave bands at 60° incidence. A new estimate of the HDR at 0° is obtained using Equation (29), the measured HDR at 20° and the average *b* parameter; this process is iterated until the HDR value at 0° converges. The mean and standard deviation in measured HDR at 20° and 60° are provided in Tables 8 through 11 for all the Quest surfaces measured with the SOC-410. The computed HDR values at 0° and the average *b* parameter are listed in Table 12. Very small and negative values of *b* indicate the following surface are likely DIFFUSE: aluminum ladder, deck (no-slip), RHIB (black rubber), and the aluminum vent. The *b* parameter obtained from the SOC-410 on the white paint is very similar to that obtained using the SOC-100. However, the value for the yellow paint is 35% lower than that obtained from the SOC-100. The average difference between the measured and modelled values of ρ* is less than 0.3%. However, there is a large discrepancy between the values of ρ* obtained for each band, especially the 0.9 - 1.1 wave band (4 to 11% at 60°). This discrepancy is illustrated in the graphs of ρ* for the white and yellow paints in Figures 20 and 21, respectively.

The SOC-100 is fitted with a blocker to absorb the specular reflection off the paint sample and allow a direct measurement of the diffuse directional reflectance (DDR). However, the SOC-410 has no such capability, therefore one must assume the nominal HDR to be either totally diffuse or specular. In the case of a specular material, we assume the the nominal reflectance to be 100% diffuse, based on the SOC-100 measurements of the paint where a large fraction of the nominal HDR is diffuse (see Figures 1 through 4). A sensitivity analysis needs to be performed on the Quest ShipIR model to determine the accuracy of the SOC-410 measurement versus the SOC-100 of the yellow and white paint.

[4] SPECULAR surface in ShipIR includes both a diffuse and specular component of reflection.

Table 8: Mean HDR measured at 20°using the SOC-410.

Material	N	0.9 - 1.1	1.9 - 2.6	3.0 - 4.0	4.0 - 5.0	3.0 - 5.0	8.0 - 12.0
white	20	0.882	0.322	0.060	0.064	0.069	0.075
yellow	18	0.608	0.249	0.050	0.069	0.091	0.068
life-raft (white)	1	0.468	0.135	0.026	0.027	0.026	0.040
aluminum ladder	3	0.369	0.354	0.088	0.134	0.176	0.080
black (anchor)	2	0.048	0.046	0.041	0.041	0.041	0.044
brown bin	4	0.074	0.046	0.043	0.043	0.044	0.055
deck (smooth)	2	0.100	0.053	0.036	0.039	0.040	0.037
deck (no-slip)	3	0.362	0.196	0.044	0.062	0.078	0.046
door (wood)	6	0.684	0.209	0.041	0.052	0.066	0.066
red locker (small)	4	0.752	0.218	0.041	0.047	0.055	0.072
red locker (large)	2	0.289	0.092	0.042	0.054	0.068	0.059
RHIB (red)	4	0.665	0.186	0.042	0.043	0.045	0.072
RHIB (black rubber)	2	0.053	0.035	0.025	0.026	0.027	0.022
aluminum vent	2	0.473	0.628	0.295	0.425	0.552	0.327
window	2	0.040	0.040	0.037	0.035	0.033	0.133

Table 9: Mean HDR measured at 60°using the SOC-410.

Material	N	0.9 - 1.1	1.9 - 2.6	3.0 - 4.0	4.0 - 5.0	3.0 - 5.0	8.0 - 12.0
white	20	0.914	0.370	0.109	0.113	0.117	0.123
yellow	18	0.648	0.291	0.091	0.105	0.124	0.117
life-raft (white)	1	0.506	0.166	0.054	0.054	0.058	0.082
aluminum ladder	3	0.392	0.351	0.077	0.115	0.151	0.069
black (anchor)	2	0.082	0.084	0.082	0.083	0.083	0.097
brown bin	4	0.106	0.082	0.086	0.087	0.087	0.105
deck (smooth)	2	0.135	0.084	0.068	0.070	0.071	0.080
deck (no-slip)	3	0.370	0.213	0.056	0.074	0.091	0.055
door (wood)	6	0.702	0.243	0.079	0.089	0.102	0.102
red locker (small)	4	0.792	0.263	0.086	0.092	0.100	0.123
red locker (large)	2	0.349	0.138	0.094	0.102	0.112	0.110
RHIB (red)	4	0.707	0.226	0.077	0.078	0.081	0.114
RHIB (black rubber)	2	0.069	0.050	0.040	0.041	0.041	0.040
aluminum vent	2	0.422	0.568	0.241	0.354	0.466	0.292
window	2	0.080	0.077	0.077	0.073	0.071	0.209

Table 10: Standard deviation in HDR measured at 20°using the SOC-410.

Material	N	0.9 - 1.1	1.9 - 2.6	3.0 - 4.0	4.0 - 5.0	3.0 - 5.0	8.0 - 12.0
white	20	0.046	0.033	0.011	0.010	0.011	0.005
yellow	18	0.030	0.102	0.017	0.057	0.109	0.006
life-raft (white)†	1						
aluminum ladder	3	0.030	0.102	0.019	0.023	0.027	0.018
black (anchor)	2	0.031	0.034	0.001	0.002	0.001	0.003
brown bin	4	0.012	0.009	0.013	0.013	0.016	0.003
deck (smooth)	2	0.014	0.007	0.006	0.006	0.007	0.001
deck (no-slip)	3	0.012	0.015	0.010	0.015	0.022	0.005
door (wood)	6	0.077	0.039	0.006	0.011	0.016	0.004
red locker (small)	4	0.034	0.021	0.011	0.012	0.014	0.009
red locker (large)	2	0.010	0.004	0.001	0.003	0.008	0.000
RHIB (red)	4	0.082	0.013	0.006	0.006	0.008	0.003
RHIB (black rubber)	2	0.007	0.001	0.003	0.000	0.001	0.005
aluminum vent	2	0.025	0.025	0.006	0.010	0.014	0.007
window	2	0.001	0.002	0.001	0.000	0.002	0.008

†Need at least 2 points to compute standard deviation.

Table 11: Standard deviation in HDR measured at 60°using the SOC-410.

Material	N	0.9 - 1.1	1.9 - 2.6	3.0 - 4.0	4.0 - 5.0	3.0 - 5.0	8.0 - 12.0
white	20	0.045	0.033	0.013	0.012	0.007	0.041
yellow	18	0.033	0.097	0.015	0.044	0.083	0.008
life-raft (white)†	1						
aluminum ladder	3	0.028	0.028	0.013	0.017	0.022	0.017
black (anchor)	2	0.003	0.002	0.001	0.001	0.001	0.001
brown bin	4	0.013	0.010	0.014	0.017	0.018	0.005
deck (smooth)	2	0.016	0.007	0.004	0.006	0.006	0.000
deck (no-slip)	3	0.011	0.015	0.011	0.017	0.023	0.006
door (wood)	6	0.079	0.043	0.010	0.015	0.021	0.010
red locker (small)	4	0.030	0.019	0.017	0.018	0.018	0.008
red locker (large)	2	0.012	0.001	0.002	0.001	0.006	0.001
RHIB (red)	4	0.079	0.017	0.014	0.013	0.014	0.011
RHIB (black rubber)	2	0.011	0.005	0.004	0.005	0.002	0.002
aluminum vent	2	0.012	0.016	0.004	0.009	0.011	0.009
window	2	0.013	0.013	0.011	0.011	0.013	0.030

†Need at least 2 points to compute standard deviation.

Table 12: Calculated HDR at 0° and average *b* values.

Material	b	0.9-1.1	1.9-2.6	3.0-4.0	4.0-5.0	3.0-5.0	8.0-12.0
white	0.0206	0.881	0.320	0.058	0.061	0.067	0.072
yellow	0.0166	0.607	0.247	0.024	0.067	0.089	0.038
life-raft (white)	0.0122	0.467	0.134	0.048	0.025	0.024	0.066
aluminum ladder	-0.0055	0.370	0.355	0.088	0.134	0.177	0.081
black (anchor)	0.0160	0.045	0.043	0.038	0.038	0.038	0.042
brown bin	0.0158	0.072	0.044	0.041	0.041	0.042	0.053
deck (smooth)	0.0129	0.098	0.051	0.034	0.037	0.038	0.035
deck (no-slip)	0.0048	0.362	0.195	0.043	0.062	0.077	0.045
door (wood)	0.0144	0.684	0.207	0.039	0.051	0.065	0.064
red locker (small)	0.0186	0.751	0.216	0.039	0.045	0.053	0.069
red locker (large)	0.0188	0.287	0.090	0.040	0.052	0.066	0.057
RHIB (red)	0.0150	0.664	0.184	0.040	0.041	0.043	0.070
RHIB (black rubber)	0.0056	0.052	0.034	0.024	0.025	0.026	0.021
aluminum vent	-0.0366	0.476	0.630	0.298	0.428	0.554	0.330
window	0.0121	0.038	0.037	0.035	0.033	0.030	0.130

shaded materials were found to be DIFFUSE.

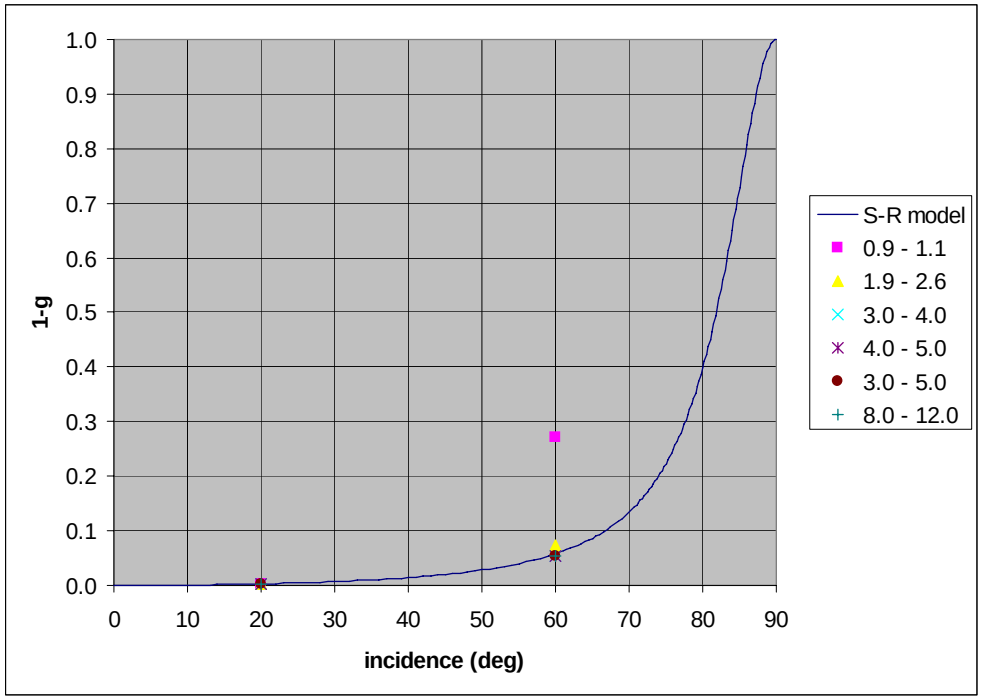

Figure 20: Plot of measured and predicted normalized reflectance for the Quest white paint.

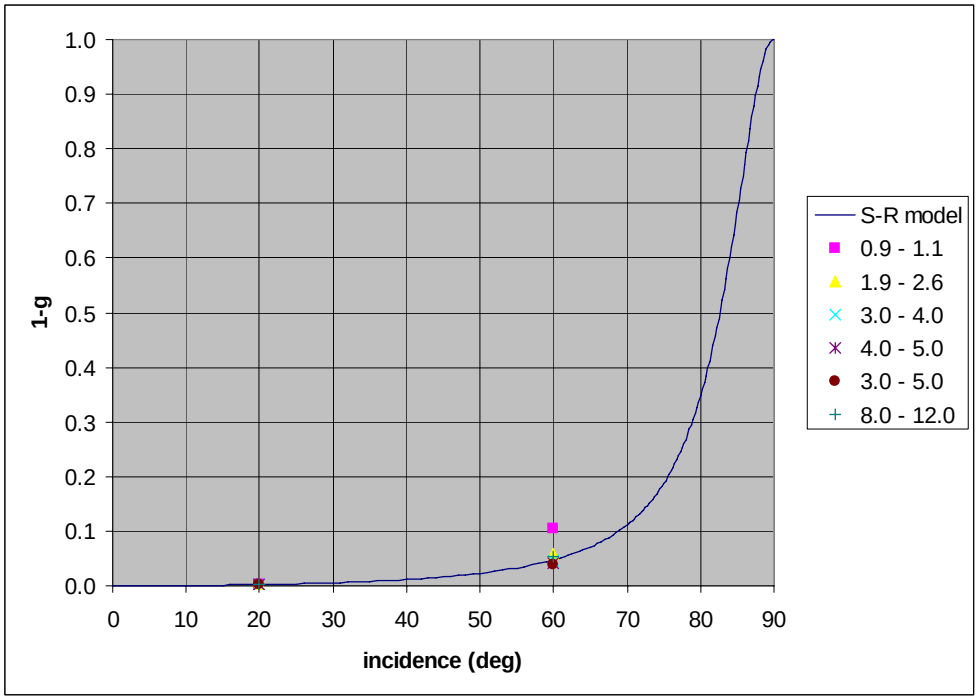

Figure 21: Plot of measured and predicted normalized reflectance of the Quest yellow paint.

4. CONCLUSION

A standard measurement and analysis procedure has been described for inputting surface properties into the ShipIR model. The following Surface Optics Corporation measurements are prescribed:

- nominal full-spectral HDR and DDR measurements at 20° or 30° incidence,
- additional HDR measurements at 50°, 60°, 70° and 80°, and
- in-plane bi-directional reflectance distribution function (BRDF) measurements at 4 and 10 μm, at 20° or 30° incidence.

The resultant output data consists of:

- solar absorptivity
- thermal emissivity
- nominal spectral emissivity
- nominal specular reflectance (NSR)
- grazing angle coefficient (*b*)
- full-width at half-maximum lobe angle (FWHM)

Sample results for the unclassified Canadian research vessel Quest show that similar results are obtained for both the data measured at 20° or 30° incidence angle. Additional HDR measurements at higher angles of incidence (50°, 60°, 70° and 80°) are used to derive an average *b* parameter for input to the model, based on the assumptions made by Sandford and Robertson (1985). Assuming the spectral and directional terms of specular reflectance to be separable, the inputs to the model are simplified, but a significant difference exists between the measured and predicted values of HDR. A standard error (2σ) of 5.4% for the white paint and 8.4% for the yellow paint was obtained. Further research is needed to determine if a better model can be formulated. For example, the complex index of refraction (n, k) could be derived and combined with the PDF model to predict the measured HDR versus wavelength and angle. A simplified version of the Cox and Munk PDF sun-glint model was used to obtain a surface roughness and lobe-width angle (FWHM) from the peak BRDF measured. The resultant

model fit the measured BRDF profile very well. The average lobe-width from the measurements at 4 and 10 μm and 20° and 30° incidence are used as input to the ShipIR model.

In-field measurements performed on Quest using a handheld SOC-410 HDR reflectometer were used to estimate the thermal and in-band surface properties of different areas on the ship. A round robin comparison of the in-band SOC-410 measurements with the full-spectral SOC-100 in-lab measurements revealed differences in HDR ranging from -6% to +7%; these far exceed the standard deviation in the recorded samples from the SOC-410 taken at different locations on the ship. The absolute difference contribute to a similar difference in the estimates of solar absorptivity and thermal emissivity. The methods used to derive a *b* parameter from the SOC-410 and SOC-100 measurements showed similar results for the white paint (b_{100}=0.023, Δ_{410}=-9%) and large differences for the yellow paint (b_{100}=0.023, Δ_{410}=-35%).

5. REFERENCES

1. Cox, C. and W. Munk. 1954. Measurement of the Roughness of the Sea Surface from Photographs of the Sun's Glitter, *J. Opt. Society Am.* 44, p. 838-850.

2. Fraedrich, D.S., E. Stark, L.T. Heen and C. Miller. 2003. ShipIR model validation using NATO SIMVEX experiment results. *Proc. SPIE* 5075:49-59, Targets and Backgrounds IX: Characterization and Representation.

3. Mermelstein, M.D., E.P. Shettle, E.H. Takken and R.G. Priest. 1994. Infrared radiance and solar glint at the ocean-sky horizon. *Appl. Opt.* 33 (25):6022-6034.

4. Sandford, B.P. and D.C. Robertson. 1985. Infrared reflectance properties of aircraft paints (U). *Proc.IRIS*: Targets, Backgrounds, and Discrimination.

5. Ship and Atmospheric Propogation Phenonmen Infrared Experiment (SAPPHIRE), NATO SET/088 RTG51 on Littoral Infrared Ship Self Defence Technology, June 2006, Chesapeake Bay, USA.

6. Vaitekunas, D.A. and D.S. Fraedrich. 1999. Validation of the NATO-standard ship signature model (SHIPIR). *Proc. SPIE* 3699: 103-113, Targets and Backgrounds: Characterization and Representation V.

7. Vaitekunas, D.A. 2002. Technical Manual For ShipIR/NTCS (v2.9), Davis Document No. A912-002, Rev 0.

8. Vaitekunas, D.A. 2004. *Infrared Signature Instrumentation, Measurement, and Modelling of CFAV Quest for Trial Q276*. Davis Document No. A320-001, Rev 0 (performed under PWGSC Contract No. W7707-3-2128).

9. Vaitekunas, D.A. 2005. Validation of ShipIR (v3.2): methods and results. Presented at the 1st International Workshop for IR Target and Background Modelling, 27–30 June, 2005. Ettlingen, Germany.

10. Vaitekunas, D.A. 2006. Modelling and analysis of ship surface BRDF. Presented at the 2nd International Workshop on IR Target and Background Modelling & Simulation, 26–29 June 2006, FGAN-FOM Research Institute for Optronics and Pattern Recognition, Ettlingen, Germany.